Experimental characterization of magnetic surface plasmons on metamaterials with negative permeability

Jonah N. Gollub,[1,2] David R. Smith,[1,2] David C. Vier,[2] Tim Perram,[2] and Jack J. Mock[1]
[1]*Department of Electrical and Computer Engineering, Duke University, Durham, North Carolina 27708, USA*
[2]*Department of Physics, University of California, San Diego, California 92037, USA*
(Received 26 October 2004; published 6 May 2005)

We study the surface plasmons (SPs) that exist at the interface between air and a metamaterial constructed of split ring resonators (SRRs). The SRR metamaterial possesses a frequency band in the microwave regime (12.5–14 GHz) over which the permeability is negative. We apply an attenuated total reflection technique in the Otto configuration in which a beam of microwaves is reflected from a higher dielectric (polycarbonate) prism to excite and probe the surface plasmons. The resulting evanescent microwave fields on the transmission side of the prism couple to SPs on the metamaterial and are indicated by a dip in the reflected power. The experimental data are compared with analytic solutions in which the metamaterial slab is approximated as an infinite half space, for which the frequency-dependent permeability (and permittivity) is derived from finite-element simulations on an SRR structure with the same parameters as those measured.

DOI: 10.1103/PhysRevB.71.195402 PACS number(s): 73.20.Mf

I. INTRODUCTION

Maxwell's equations predict the existence of propagating electromagnetic modes, often called surface plasmons (SPs), at the interface between two materials with oppositely signed permittivity ϵ or permeability μ. SPs on materials with negative ϵ were predicted and demonstrated in the 1950s,[1] and have since been extensively studied in a variety of contexts.[2] The most commonly known materials that support SPs are the noble metals–silver and gold, for example. In these and in many other metals the frequency-dependent dielectric function is approximately free-electron-like, characterized by a plasma frequency [usually in the ultraviolet (UV)], below which ϵ is negative. Because the plasma frequency for most metals is in the UV, SPs naturally tend to occur at wavelengths ranging from UV to visible.

The plasmon represents a coupling of the electromagnetic field with the conduction electrons in a metal. In a SP, charge-density oscillations occur just along the interface of the metal and a second material whose $\epsilon > 0$. The SP is bound to and propagates along this interface. The SP modes can also occur on textured metallic surfaces, such as gratings, where their dispersion properties can be tuned by adjusting the surface patterning.[3] Textured conducting surfaces or structured conducting materials can drastically change the frequency range over which SP modes occur; in particular, the surface properties can predominate over the inherent material properties, such that SPs can be observed at microwave frequencies on suitably designed conducting gratings.[4]

Surface plasmons have long been appreciated for their ability to localize light to a scale not restricted by the wavelength. The resulting localized fields usually exhibit large enhancements over the incident field, making SPs useful probes of their local environments. The extreme sensitivity of the SP on gold films, for example, has been used as the basis for highly sensitive biochemical sensors.[5–7] With the current expansion of nanofabrication efforts, the ability to form tailored structures has furthered interest in plasmonic structures as optical tools to guide and manipulate light.[8–10]

While there has been considerable analysis and application development of electric SP structures—those which require a material with negative ϵ, it is also possible for SPs to occur between two materials having opposite signs of μ. Naturally occurring systems, such as resonant ferromagnets and antiferromagnets exhibit a band of negative μ just above the resonant frequency.[11] A convenient method for probing the properties of a negative μ frequency band is to excite magnetic SPs and characterize their dispersion.[12] The difference between magnetic and electric SPs is that effective magnetic surface charges rather than electric surface charges participate in the coupled electromagnetic mode. In general, electric SPs will have *p*-polarized electromagnetic fields (magnetic field perpendicular to propagation) while magnetic SPs will have *s*-polarized electromagnetic fields (electric field perpendicular to propagation).

There has been little exploration of magnetic SPs, as the number of available materials with negative μ and the frequency range over which they are available are considerably smaller than for materials with negative ϵ. However, since the surface properties of gratings or other structured materials can be significantly distinct from the underlying constituent materials, it might be expected that artificially patterned structures would support magnetic SPs. Over the past several years, there has been a renewed interest in the development of artificial materials to achieve electromagnetic responses that are difficult or impossible to achieve in conventional materials. A periodic array of conducting wires, for example, can be characterized via effective medium theory as having an ϵ with the same plasmonic form as silver, but with a plasma frequency determined by the wire radius and spacing.[13] Wire structures have been fabricated that have effective plasma frequencies in the microwave regime,[14] and which have been shown to support electric SPs.[15]

In 1999, it was suggested that an array of planar conducting, resonant elements, termed split ring resonators (SRRs), could behave as an artificial medium with a predominantly magnetic response to incident electromagnetic radiation.[16] The electromagnetic properties of the composite structure

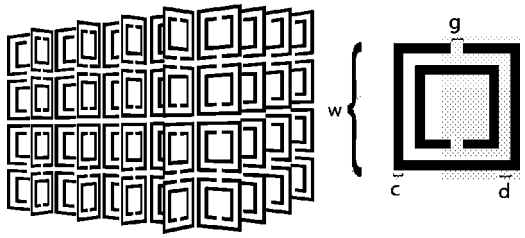

FIG. 1. A metamaterial structure was constructed out of sheets of SRRs assembled into a three-dimensional (3D) structure. The rings counterpose one another to satisfy the boundary conditions of the waveguide in which the experiment was performed. The characteristic dimensions of the SRRs are shown. The values for the sample considered in this paper are $w=2.14$ mm, $c=0.13$ mm, $d=0.35$ mm, and $g=0.47$ mm. Each unit cell is 2.5 mm $\times$ 2.5 mm $\times$ 2.5 mm.

can be described by a frequency-dependent μ similar in form to the Drude-Lorentz model, with a resonant frequency ω_0 and a magnetic plasma frequency ω_{mp} where $\mu=0$. If the SRRs are placed close enough together, and the losses in the conductors are reasonably low, then the effective oscillator strength of the SRR medium can be large enough that the effective μ is negative above ω_0 and below ω_{mp}. The negative μ response of the SRR medium was demonstrated in the context of a negative index metamaterial,[17] in which the SRR medium was combined with a wire medium to produce a composite for which both ϵ and μ were negative over a range of microwave frequencies. Since that demonstration, the properties of the SRR medium have been further studied[18] and thoroughly analyzed.[19–22]

Our goal here is to explore the excitation of SPs on a magnetic metamaterial composed of a SRR array. The SRR medium is designed such that the effective permeability μ is negative over a band of frequencies in the microwave regime. The occurrence of magnetic SPs at the interface of an artificially structured metamaterial, simply and correctly described by a Drude-Lorentz model, illustrates the utility of the metamaterials approach to realizing phenomena difficult to achieve in conventional materials. In studying the magnetic SPs here at microwave frequencies, we apply the same techniques used to excite SPs on thin metal films at optical wavelengths.

II. THEORY

The metamaterial that we utilize is composed of a collection of SRR resonators positioned periodically as shown in Fig. 1. An essential feature of a metamaterial is that the size and spacing of the SRR resonators is significantly smaller than the wavelengths of interest—on the order of 3 cm at *X*-band frequencies (8–12 GHz). With this constraint fulfilled, the resulting electromagnetic response of the spatially inhomogeneous composite approximates that of a continuous material. The generic form of the permeability of the SRR medium has been found to have the resonant form,[16]

$$\mu(\omega) = 1 - \frac{F\omega^2}{\omega^2 - \omega_0^2 + i\Gamma\omega}, \tag{1}$$

indicating a band of frequencies between ω_0 and $\omega_{\mathrm{mp}} = \omega_0/\sqrt{1-F}$ where μ is negative (for small Γ). We thus expect that in this frequency range the SRR medium will support magnetic SPs.

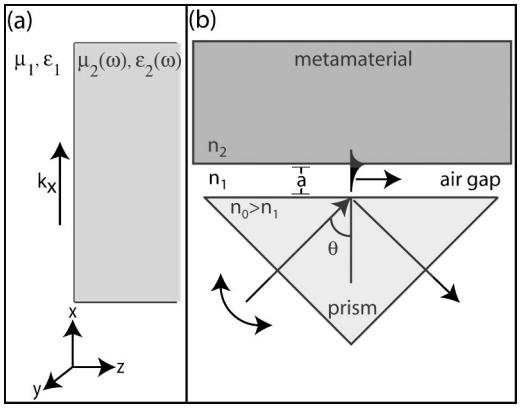

FIG. 2. (a) *s*-polarized SPs move along the infinite half-space boundary between a material with μ_1 and ϵ_1 and a metamaterial with frequency dependent $\mu_2(\omega)$ and $\epsilon_2(\omega)$. (b) To excite surface plasmons, an Otto attenuated total-reflection (OATR) technique is used. Radiation is incident on the boundary of a prism and medium of lesser index of refraction (air in our case). The incident angle of the radiation is greater than the critical angle for total internal reflection, resulting in an evanescent field decaying away from the prism. The metamaterial is close to (but not touching) the prism at a distance *a*. The evanescent field above the prism couples to surface plasmons on the metamaterial and causes a dip in the reflected power from the prism boundary.

To model the expected characteristics of the SPs, we first consider an infinite half space of material in the region $z>0$, [see Fig. 2(a)]. We assume that the material has an isotropic frequency-dependent permeability $\mu_2(\omega)$. For generality, we also assume that the material has a frequency-dependent permittivity $\epsilon_2(\omega)$, even though we expect much less variation in the permittivity for the SRR medium considered here. For $z<0$, we assume constant $\epsilon_1 \geqslant 1$ and $\mu_1 \geqslant 1$. Because we will be assuming magnetic SPs, and to be consistent with the experiments presented later, we analyze the case of *s*-polarized SPs. The general solution in the two half spaces for the propagating modes has the form $\mathbf{E_j} = (0, E_{y_j}, 0)e^{i(k_{x_j}x \pm k_{z_j}z - \omega t)}$ and $\mathbf{H_j} = (H_{x_j}, 0, H_{z_j})e^{i(k_{x_j}x \pm k_{z_j}z - \omega t)}$ where $(j=1,2)$ refers to either vacuum or material, respectively. Phase matching requires $k_{x_1} = k_{x_2} \equiv k_x$.

From the scalar wave equation $[\nabla^2 + \epsilon_j\mu_j(\omega/c)]E_y = 0$, we can derive the dispersion relation in the two regions,

$$k_x^2 = \epsilon_j\mu_j\left(\frac{\omega}{c}\right)^2 - k_{z_j}^2. \tag{2}$$

At the interface, the tangential components of the electric and magnetic fields E_y, H_x must be continuous, yielding[2]

$$\mu_2 k_{z_1} = -\mu_1 k_{z_2}. \tag{3}$$

Solving for k_x using Eqs. (2) and (3), we find

$$k_x = \frac{\omega}{c}\sqrt{\frac{\mu_1\mu_2(\epsilon_1\mu_2 - \epsilon_2\mu_1)}{\mu_2^2 - \mu_1^2}}, \tag{4}$$

which simplifies further when $\epsilon_1 = \mu_1 = 1$ to

$$k_x = \frac{\omega}{c}\sqrt{\frac{\mu_2(\mu_2 - \epsilon_2)}{\mu_2^2 - 1}}. \tag{5}$$

For a lossless medium with $\epsilon_2 = +1$, inspection of Eq. (5) shows that in the frequency range where $\mu_2 < -1$, $k_x > \omega/c$. This result, combined with Eq. (2), implies that k_{z_1} and k_{z_2} are both imaginary. Consequently, the electromagnetic field decays exponentially away from both sides of the interface. This SP mode is thus strictly bound to the interface, propagating along the surface with propagation constant k_x.

Because SP modes have $k_x > \omega/c$, they cannot be matched to propagating modes incident from free space, and thus cannot be excited by plane-wave excitation. A well-known method for coupling incident radiation to SPs is the Otto attenuated total-reflection (OATR) technique,[2,23] shown schematically in Fig. 2(b). A beam of radiation is incident from vacuum (index of n_1) through one face of a high-index prism with index $n_0 \geqslant n_1$. The beam passes through the prism and is incident on a second interface at some angle. For angles greater than a critical angle, the beam undergoes a total internal reflection at the second interface and exits the prism at the third interface. At the surface of the reflection interface, a decaying evanescent wave exists on the vacuum side of the prism, for which the parallel component of the wave vector $k_x > \omega/c$. When the metamaterial is brought close to (but not touching) the prism, this evanescent wave can couple to the SP mode. A minimum is observed in the power reflected from the prism/air interface at the frequency at which the parallel component of the wave vector of the incident wave matches the k_x of the SP.

The analysis thus far presented assumes that the material occupies an infinite half space, whereas the metamaterial used in the experiments is of finite thickness. However, for slabs of sufficient thickness, the SPs on either side of the slab are essentially decoupled due to material losses so that the infinite half-space analysis applies.

A. OATR reflection coefficient

To calculate the reflection coefficient for an OATR experimental setup, we assume an incoming *s*-polarized plane wave of the form $\mathbf{E} = E_{0R} e^{i(\mathbf{k}_0 \cdot \mathbf{r} - \omega t)}$. The general solution in each region is $E_{jR} e^{i(\mathbf{k}_j \cdot \mathbf{r} - \omega t)} + E_{jL} e^{i(-\mathbf{k}_j \cdot \mathbf{r} - \omega t)}$, where $j = 0, 1, 2$ (prism, gap, metamaterial, respectively) refers to the region of interest. The wave equation for *s*-polarized waves is scalar and can be parametrized in terms of the *y* component of the electric field in each region. Let a be the separation distance between the prism and the metamaterial. Applying boundary conditions at $x = 0$ and $x = a$ leads to the following set of equations:

$$E_{y_{0R}} + E_{y_{0L}} = E_{y_{1R}} + E_{y_{1L}}, \tag{6}$$

$$\frac{1}{\mu_0} k_{z_0}(-E_{y_{0R}} + E_{y_{0L}}) = \frac{1}{\mu_1} k_{z_1}(-E_{y_{1R}} + E_{y_{1L}}), \tag{7}$$

$$E_{y_{1R}} e^{ik_{z_1}a} + E_{y_{1L}} e^{-ik_{z_1}a} = E_{y_{2R}} e^{ik_{z_2}a}, \tag{8}$$

$$\frac{1}{\mu_2} k_{z_2}(-E_{y_{1R}} e^{ik_{z_2}a}) = \frac{1}{\mu_1} k_{z_1}(-E_{y_{1R}} e^{-ik_{z_1}a} + E_{y_{1L}} e^{-ik_{z_1}a}). \tag{9}$$

The wave number k_{z_j} follows from the dispersion relation [Eq. (2)] and the continuity of k_x,

$$k_{z_0} = \frac{\omega}{c}[n_0^2 - n_0^2 \sin^2(\theta_0)]^{1/2}, \tag{10}$$

$$k_{z_1} = \frac{\omega}{c}[n_1^2 - n_0^2 \sin^2(\theta_0)]^{1/2}, \tag{11}$$

$$k_{z_2} = \frac{\omega}{c}[\mu_2(\omega)\epsilon_2(\omega) - n_0^2 \sin^2(\theta_0)]^{1/2}. \tag{12}$$

Given the $\mu_2(\omega)$ and $\epsilon_2(\omega)$ functions for the metamaterial and the index of refraction of the prism and dielectric n_0 and n_1 we have a set of equations that can be solved for the reflected electric-field component $E_{y_{0L}}$ in terms of the angular frequency ω, the separation distance a, and the incident angle θ_0. We then obtain a numerical solution from these equations using MATHEMATICA (Wolfram Research).

The reflectance $R(\omega)$ or normalized reflected power from the surface of the prism is given by

$$R(\omega) \equiv \frac{\langle S_{0L} \rangle \cdot (-\hat{\mathbf{x}})}{\langle S_{0R} \rangle \cdot \hat{\mathbf{x}}} = \frac{|E_{y_{0L}}|^2}{|E_{y_{0R}}|^2}, \tag{13}$$

where S is the Poynting vector. The metamaterials considered in this paper have negative $\mu_2(\omega)$ and positive $\epsilon_2(\omega)$. With these parameters we can expect the SPs on these materials to show up as dips in $R(\omega)$ in the frequency range where $\mu_2(\omega)/\mu_1 < -1$.

B. Numerical simulation

While the generic form for the frequency-dependent permeability for the SRR medium, Eq. (1), has been shown to qualitatively describe the SRR medium, the numerical results obtained from using this approximate expression are unlikely to be quantitatively correct for the fabricated SRR structure. Accurate values for the frequency dependent μ and ϵ can be obtained from numerical solutions of the electromagnetic modes corresponding to a single unit cell of the composite SRR structure. The dimensions of the SRRs corresponding to the structure used in the measurements are indicated in Fig. 1. The structure, designed to be isotropic in a plane, consists of SRRs periodically repeated in two orthogonal directions. The SRRs are assumed to be deposited with a thickness of 0.017 mm on a circuit board substrate with a dielectric constant of 4.07. All aspects of the geometry and material characteristics of the unit cell are included in the finite-element numerical simulations, performed using HFSS (Ansoft).

To determine the ϵ and μ functions, a unit cell of the metamaterial is simulated, with periodic boundary conditions applied in the directions perpendicular to propagation. The complex transmission and reflection coefficients (or scatter-

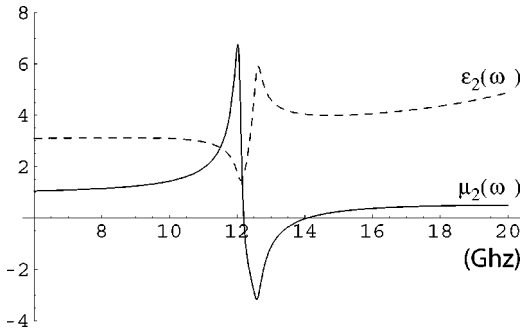

FIG. 3. The real parts of the permeability $\mu_2(\omega)$ and permittivity $\epsilon_2(\omega)$ of the metamaterial are shown. They are derived from the numerical simulations of split rings using Ansoft's HFSS software.

ing parameters) are then calculated, from which the values of ϵ and μ can be extracted.[15,24] The result of this process yields the functions shown in Fig. 3. Utilizing these forms in Eq. (5), we can accurately determine the frequency dispersion of the SP modes for the SRR metamaterial.

The theoretical dispersion curve for the SRR medium can also be calculated using the finite-element numerical simulation. A dispersion diagram is shown in Fig. 4. The gap in transmissive propagating modes over the frequency range of 12–14 Ghz corresponds to the region where $\mu_2(\omega)$ is negative. It is in this region that we expect to find the propagating surface modes or SPs experimentally.

III. EXPERIMENT

A convenient method for characterizing the scattering properties of a metamaterial sample is to place the sample in a planar-waveguide scattering chamber. For a planar waveguide formed by two conducting sheets, the lowest TE mode has no cutoff frequency and is characterized by uniform fields; the electric field is polarized perpendicular to the plates and the magnetic field is polarized parallel to the plates. In effect, the lowest TE mode is equivalent to a free-space *s*-polarized plane wave. As long as the scattering elements that form the metamaterial sample possess reflection symmetry about the center plane between the upper and the lower waveguide plates, the equivalence of the waveguide modes to the *s*-polarized free-space waves is maintained.

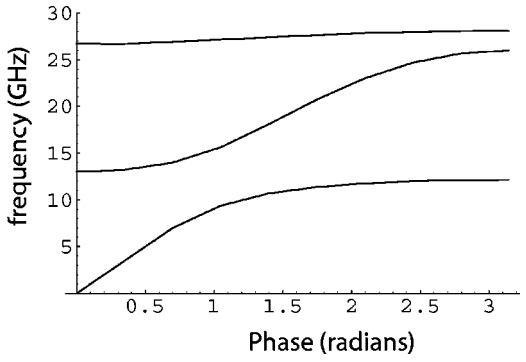

FIG. 4. Numerical simulation of the transmission-dispersion relation through the metamaterial done in Ansoft's HFSS software by modeling the structure of the split ring cells. The horizontal axis is the phase advance per unit cell or *kd*, where *k* is the wave number (2π divided by the free-space wavelength) and *d* is the SRR cell width.

An angle-resolved microwave spectrometer (ARMS) has been previously built to enable planar waveguide measurements on metamaterial samples.[25] Microwaves are generated and detected in the ARMS apparatus by an Agilent vector network analyzer (model 8722ES). The microwave energy is injected as an apertured beam via an extended arm connected to the flat side of a semicircular planar waveguide chamber (plate separation of 1 cm). The metamaterial sample is placed at the center of the plates, and it scatters the incoming beam. The ARMS apparatus allows the scattered power to be detected around the waveguide periphery by means of a waveguide detector placed on a rotatable arm.

Because the ARMS apparatus allows *s*-polarized wave propagation solely in the plane of the waveguide, it is necessary to construct a metamaterial for which the μ response is negative in only two dimensions (the magnetic properties in the third dimension are not sensed by these waves). A metamaterial sample patterned in two rather than three dimensions significantly eases the sample fabrication burden.

The metamaterial constructed for this experiment consists of a two-dimensional (2D) grid of SRR cells, as shown schematically in Fig. 1. A photolithography process was used to fabricate the SRR structure. The split ring design, also shown in Fig. 1, was drawn in ADOBE ILLUSTRATOR. A mask of the design was printed on a transparency with a 600 dpi laser printer. A single-sided copper-clad FR4 circuit board, concealed by a layer of photoresist, was covered by the mask and exposed to ultraviolet light for 1 min, then put in a developer solution (sodium carbonate) and agitated. Next the board was placed in etching solution (ferric chloride) for 1 h during which its orientation was altered every 15 min to ensure even etching. Finally, the board was placed in a stripper solution (potassium hydroxide) for about 10 min. After drying, a ProtoMatC100/HF milling machine was used to cut the circuit board into strips, 4 cells in height and 100 cells in length. Notches were cut between cells, allowing the strips to be assembled together in a three-dimensional (physical) structure. The patterns for the notches and the cutout were also drawn in ILLUSTRATOR and processed using CIRCUITCAM and BOARDMASTER software (LPKF). For this experiment, the SRRs were assembled into a $13\times3.5\times1$-cm rectangular slab.

To confirm that the simulated properties of the SRR metamaterial were consistent with those of the fabricated structure, a comparison was made between the simulated and measured transmitted power through the metamaterial slab, as shown in Fig. 5. The measured power spectrum revealed a 3.6-GHz-wide region of attenuation over the frequency range of 10.4–14 Ghz. The observed gap, over which μ was presumably negative, was in excellent agreement with the simulated transmission spectrum obtained from the numerical simulations. The agreement suggests that the simulations have accurately described the properties of the SRR metamaterial.

The recovered functional forms for $\mu_2(\omega)$ and $\epsilon_2(\omega)$ were used to solve numerically for the reflectance, as described in

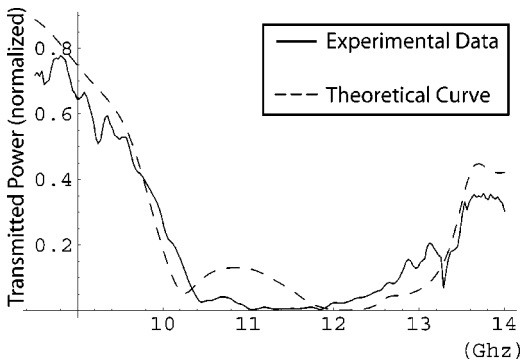

FIG. 5. The normalized experimental and numerically simulated power transmitted through the metamaterial are shown versus frequency. The numerical simulation is done using Ansoft's HFSS software by modeling, in the direction of propagation, a ten-cell-thick split-ring structure sandwiched between 1 cm metal plates.

Sec. II A. Figure 6 shows the predicted SP resonance for an incident angle $\theta_0 = 45°$ and a range of separation distances a between the prism and the metamaterial.

To characterize the SPs, an OATR experiment is performed. A 1-cm-thick $45° \times 45°$ right triangular prism constructed out of polycarbonate is used, for which the index of refraction of the prism is $n_0 = 1.63$. The s-polarized electromagnetic radiation is directed normally onto one face of the prism, encountering the second surface of the prism at an angle of $\theta_0 = 45°$. The reflected radiation then exits the third surface at normal incidence. The reflected power versus frequency is then measured by the vector analyzer (see Fig. 2) and used to normalize subsequent data. When the metamaterial is brought close to the prism, the radiation is coupled to the SPs on the metamaterial, as described above, resulting in a dip in the power spectrum.

Figure 7 shows the results of the OATR experiments for several separation distances between the metamaterial

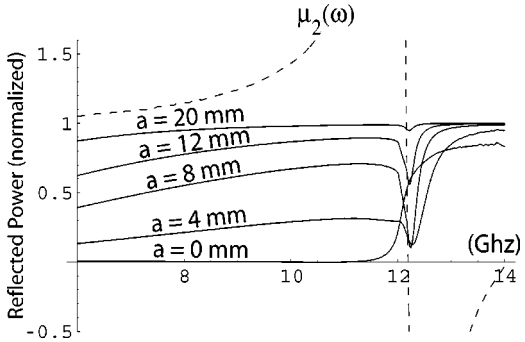

FIG. 6. The simulated, normalized reflected power for several prism/metamaterial separations a and the permeability of the metamaterial $\mu_2(\omega)$ are shown versus frequency. For incident radiation on the prism/air interface $\theta_{inc} > \theta_{TIR}$, yet there is not a total reflection of the incident radiation. In the frequency range that $\mu(\omega) > 1$ the prism/metamaterial have closely matched indexes of refraction, and the evanescent field in the gap provides a means of resonant light tunneling across the gap to the metamaterial. In the region that $\mu < -1$ the evanescent field couples to the SPs. The evanescent field strength at the surface of the metamaterial falls off as the separation distance increases, resulting in decreased coupling to the above modes (i.e., increased reflected power).

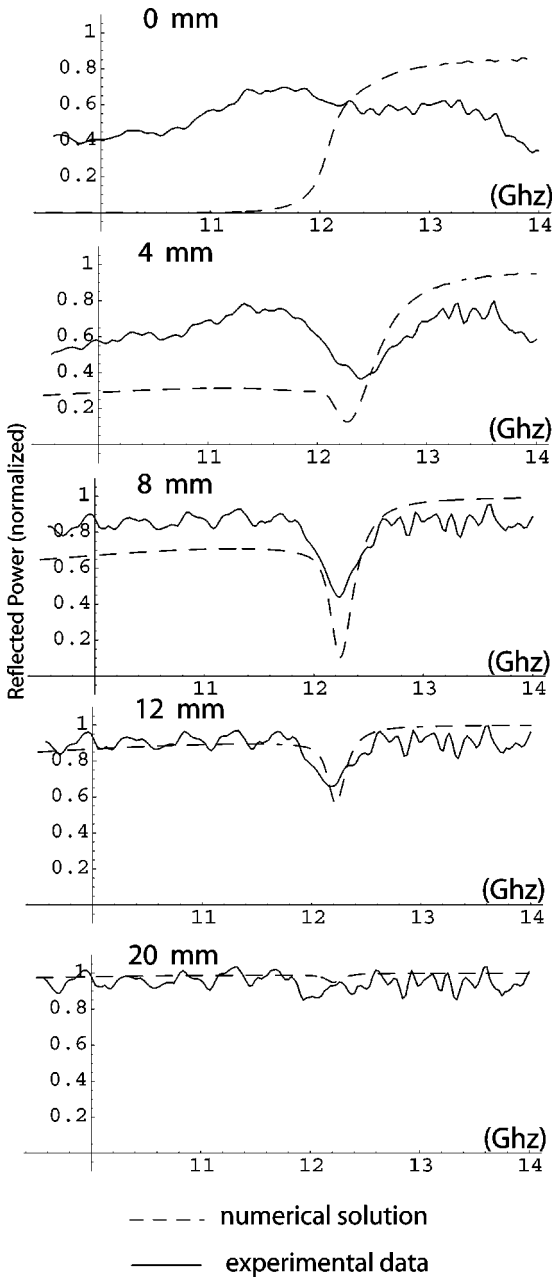

FIG. 7. The experimental data and numerical solution for the reflected power (normalized) as a function of the separation distance between the metamaterial and prism.

sample and the prism, along with the numerically computed reflection spectrum. There is a consistency between the data and the simulated solutions. The strength of the evanescent field is stronger at the metamaterial surface for the shorter separation distances, resulting in an increased coupling between the incident radiation and the SPs at small a. This can be seen in the data as the larger dip in the reflected power. The trend of increased coupling with shorter distance continues until the sample comes extremely close to the prism or touches it; in these cases, the sample either matches the prism so that transmission occurs, or it acts to reflect the incident radiation entirely.

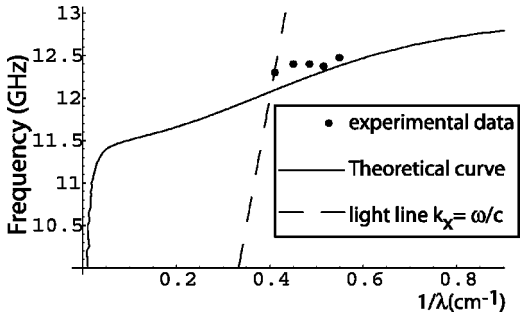

FIG. 8. The experimental surface dispersion relation for several k_x values, the theoretical dispersion relation, and the light line $k_x = \omega/c$ are shown.

There is a discrepancy between the simulated and measured data for smaller separation distances. For a uniform material we would expect the characteristic reflected power to be that of a single metamaterial/prism interface when $a = 0$, as calculated in the theory plot. The experimental data do not reflect this, drifting away from the theory plot at lower frequencies. We suspect that this inconsistency is the result of the metamaterial not being truly homogenous and so preventing a true boundary. Even at $a = 0$, the discrete size of the SRR cells makes the boundary between the prism/metamaterial poorly defined.

We can also calculate the dispersion relation for the SPs, i.e., the frequency versus resonant k_x. When we vary the incident angle of the radiation on the prism/air interface we change the k_x of the evanescent wave. The relation between the wave vector and incident angle is

$$k_x = n_0 \sin(\theta_0)\frac{\omega}{c}. \tag{14}$$

We map out the dispersion relation, k_x vs ω, by varying the incident angle over a range of values and measuring the resonant frequency of the SPs.

We must also account for the refraction of the radiation when the radiation enters the prism—it no longer enters at a normal incidence. With another application of Snell's Law we can write k_x as a function of the entering angle θ_{ent},

$$k_x = n_0 \sin\left\{\frac{\pi}{4} + \sin^{-1}\left[\frac{\sin(\theta_{\text{ent}})}{n_0}\right]\right\}\frac{\omega}{c}, \tag{15}$$

where we have set the index of refraction of our boundary material to unity, because it is air in our experiment.

The experimental data for several k_x values are shown in Fig. 8. The calculated theoretical curve, found using the HFSS data for $\mu(\omega)$ and $\epsilon(\omega)$, is also plotted along with the light line ($k_x = \omega/c$). We see that there is reasonable agreement with the theoretical curve.

IV. CONCLUSION

The results of these experiments show that a structured metamaterial can support magnetic surface plasmons, whose properties are consistent with the composite being assigned averaged electromagnetic-material parameters. The simplicity afforded by this description allows for a very convenient comparison between these magnetic SP modes and the electric SP modes that have been studied in depth at optical wavelengths over the past several decades. The metamaterial was constructed from individual SRR circuit elements; however, aside from the metamaterial boundary being somewhat ill-defined—an effect that becomes manifest when the metamaterial is closely coupled to the exciting prism—our results indicate that the measured surface properties are consistent with the composite being treated conceptually as an effective medium with homogenous electromagnetic properties. In particular, the numerical simulations of the SRR elements provided anticipated values for the effective $\mu(\omega)$ and $\epsilon(\omega)$ functions, which were then used within the standard theoretical treatment of surface plasmons on a homogenous material. The resulting agreement between the models and measurements confirms the applicability of the metamaterial approach.

An alternative approach for calculating the various modes in an SRR medium has been suggested by Shamonina *et al.*,[26] who treat the structure as a collection of periodically spaced, coupled capacitive loops. Their analysis has suggested that other modes may exist, including both propagating and surface modes. In our experiments we did not find evidence for such modes, indicating that the metamaterials analysis correctly describes the SRR medium's properties. Presumably, a method of excitation could be found that would allow the investigation of these other predicted modes, to better determine when the artificial medium's limit breaks down.

The good agreement found between the measured SRR structures and the analytical results, assuming a continuous medium, indicates that the surface mode structure of negative index metamaterials can now be probed. Combining the SRR metamaterial with a thin wire structure can produce a material that has frequency regions where both the permittivity and the permeability are negative. The surface-mode structure of such a material is quite different from and more complex than the structure presented here.[27,28]

As noted earlier, our theoretical investigation was based on an infinite half space of metamaterial and is valid to even relatively small widths of the metamaterial block (on the order of several wavelengths of the radiation). It would be of interest to investigate, both theoretically and experimentally, metamaterial strips that are thin enough so that the evanescent field inside the metamaterial does not decay before it reaches the back surface of the metamaterial. In such a case we would expect to observe joint surface plasmon excitations on both the front and back surfaces.

ACKNOWLEDGMENTS

This work was supported by a Multiple University Research Initiative (MURI) sponsored by the Army Research Office (Contract No. W911NF-04-1-0247), and a MURI sponsored by the Naval Research Office (Contract No. N00014-01-1-0803).

[1] R. H. Ritchie, Phys. Rev. **106**, 874 (1957).
[2] H. Raether, *Surface Plasmons* (Springer-Verlag, Berlin, 1988).
[3] A. P. Hibbins and J. R. Sambles, J. Appl. Phys. **86**, 1791 (1999).
[4] W. L. Barnes, A. Dereux, and T. W. Ebbesen, Nature (London) **424**, 824 (2003).
[5] J. Homola, S. S. Yee, and G. Gauglitz, Sens. Actuators B **54**, 3 (1999).
[6] R. L. Rich and D. G. Myszka, J. Mol. Recognit. **13**, 388 (2000).
[7] M. A. Cooper, Nat. Rev. Drug Discovery **1**, 515 (2002).
[8] T. W. Ebbesen, H. J. Lezec, H. F. Ghaemi, T. Thio, and P. A. Wolff, Nature (London) **391**, 667 (1998).
[9] J. C. Weeber, A. Dereux, C. Girard, J. R. Krenn, and J. P. Goudonnet, Phys. Rev. B **60**, 9061 (1999).
[10] J. D. Kottmann, O. J. F. Martin, D. R. Smith, and S. Schultz, Chem. Phys. Lett. **341**, 1 (2001).
[11] G. Suran, M. Naili, H. Niedoba, F. Machizaud, O. Acher, and D. Pain, J. Magn. Magn. Mater. **192**, 443 (1999).
[12] M. R. F. Jensen, S. A. Feiven, T. J. Parker, and R. E. Camley, Phys. Rev. B **55**, 2745 (1997).
[13] J. B. Pendry, A. J. Holden, W. Stewart, and I. Youngs, Phys. Rev. Lett. **76**, 4773 (1996).
[14] J. B. Pendry, A. J. Holden, D. J. Robbins, and W. J. Stewart, J. Phys.: Condens. Matter **10**, 4785 (1998).
[15] D. Smith, R. C. Vier, W. Padilla, S. C. Nemat-Nasser, and S. Schultz, Appl. Phys. Lett. **75**, 1425 (1999).
[16] J. B. Pendry, A. J. Holden, D. J. Robins, and W. J. Stewart, IEEE Trans. Microwave Theory Tech. **47**, 2075 (1999).
[17] D. R. Smith, W. J. Padilla, D. C. Vier, S. C. Nemat-Nasser, and S. Shultz, Phys. Rev. Lett. **84**, 4184 (2000).
[18] D. R. Smith, S. Scultz, P. Markos, and C. M. Soukoulis, Phys. Rev. B **65**, 195104 (2002).
[19] R. Marqués, F. Medina, and R. Rafii-El-Idrissi, Phys. Rev. B **65**, 144440 (2002).
[20] M. Bayindir, K. Aydin, E. Ozbay, P. Markos, and C. M. Soukoulis, Appl. Phys. Lett. **81**, 120 (2002).
[21] P. Markos and C. M. Soukoulis, Phys. Rev. E **65**, 036622 (2002).
[22] P. GayBalmaz and O. J. F. Martin, J. Appl. Phys. **92**, 2929 (2002).
[23] A. Otto, Z. Phys. **216**, 398 (1968).
[24] C. G. Parazzoli, R. B. Greegor, K. Li, B. E. C. Koltenbah, and M. Tanielian, Phys. Rev. Lett. **90**, 107401 (2003).
[25] A. F. Starr, P. M. Rye, J. J. Mock, and D. R. Smith, Rev. Sci. Instrum. **75**, 820 (2004).
[26] D. Shamonina, V. A. Kalinin, K. H. Ringhofer, and L. Solymar, J. Appl. Phys. **92**, 6252 (2002).
[27] R. Ruppin, J. Phys.: Condens. Matter **13**, 1811 (2001).
[28] R. Ruppin, Phys. Lett. A **277**, 61 (2000).